J. Fluid Mech. (1999), *vol.* 383, *pp.* 175–195. Printed in the United Kingdom

On reduction of turbulent wall friction through spanwise wall oscillations

By M. R. DHANAK AND C. SI

Department of Ocean Engineering, Florida Atlantic University, Boca Raton, FL 33431, USA

(Received 29 September 1997 and in revised form 22 October 1998)

A model for turbulent skin friction, proposed by Orlandi & Jimenez, involving consideration of quasi-streamwise vortices in the cross-stream plane, is used to study the effect on the skin friction of oscillating the surface beneath the boundary layer in the spanwise direction. Using an exact solution of the Navier–Stokes equations, it is shown that the interaction between evolving, axially stretched, streamwise vortices and a modified Stokes layer on the oscillating surface beneath, leads to reduction in the skin friction, the Reynolds stress and the rate of production of kinetic energy, consistent with predictions based on experiments and direct numerical simulations.

1. Introduction

Experimental and direct-numerical-simulation (DNS) studies suggest that coherent quasi-streamwise vortices in the wall region of a turbulent boundary layer play a significant role in the development of shear stress and turbulence production in the boundary layer. Robinson (1991) has presented a conceptual view of the type of structures frequently observed in a turbulent boundary layer. In the near-wall region, the coherent structures are dominantly quasi-streamwise, occurring singly or in pairs, the former being more frequent. These coherent structures occur intermittently in time and space, but they are the principal contributors to averaged flow quantities and therefore play an important role in the statistics of the near-wall turbulence. Although the processes governing the fluid motion in a turbulent boundary layer, including the generation of these quasi-streamwise coherent structures, are fully three-dimensional (see Schoppa & Hussain 1997, for example), crucial aspects of the interaction of these structures with the wall surface are fairly well described by the motion in the cross-plane. Orlandi & Jimenez (1994) presented a two-dimensional conceptual model which captures these aspects of the interaction in the near-wall region. The model involves consideration of the local solutions of the Navier–Stokes equations and is based on the assumption that the spatial variation of a quasi-streamwise vortex along its length is much slower than the characteristic variation in the transverse, cross-stream, plane. Thus, sufficiently fast phenomena can be studied locally in a two-dimensional plane by neglecting, in the first instance, the variation in the longitudinal direction. Using the model, they predicted the formation of the low-speed streaks and the amplification of the skin-friction owing to the presence of the streamwise vorticity. Previously, Orlandi & Jimenez (1991) took an approximate account of the influence of a straining flow, induced by larger-scale outer eddies, for example, on the interaction in their consideration; the straining flow has the effect of stretching the vortices axially, intensifying the associated vorticity, as well as moving the coherent vortices closer to the wall, thereby accentuating the interaction.

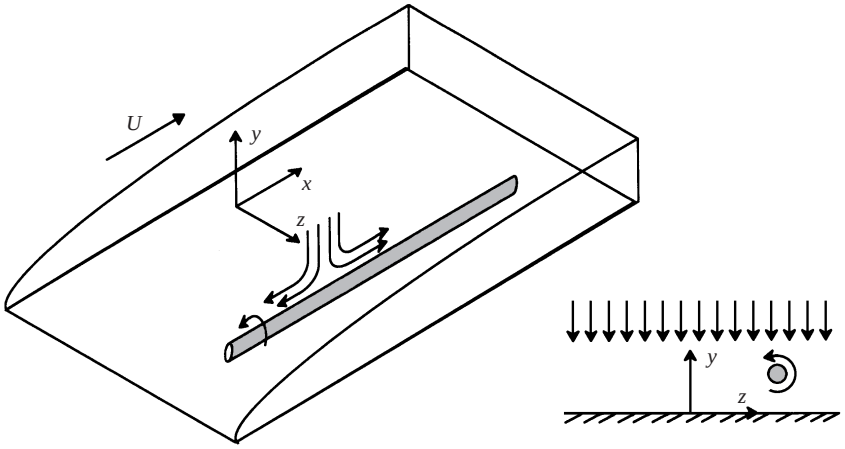

FIGURE 1. Schematics of the model flow.

In this paper, we exploit the cross-plane model of Orlandi & Jimenez to examine aspects of turbulent boundary-layer control, involving spanwise motion of the wall. Our approach is similar to theirs except that we take full account of vortex stretching by incorporating an appropriate modification to their vorticity-streamfunction formulation. Allowing for the vortex stretching renders the flow three-dimensional. The formulation has a disadvantage in terms of computational time used, but allows proper consideration of the influence of the straining flow, using an exact solution of the Navier–Stokes equations.

Several recent experimental and direct numerical simulation studies (Bradshaw & Pontikos 1985; Moin *et al.* 1990; Jung, Mangiavacchi & Akhavan 1992; Laadhari, Skandaji & Morel 1994; Choi & Clayton 1998) have shown that imposition of an oscillatory spanwise pressure gradient or spanwise oscillation of the wall beneath the boundary layer, temporarily inhibits production of turbulence in the flow, leading to transient reductions in all turbulent quantities including the Reynolds shear stress and the rate of production of turbulent kinetic energy. In particular, in a direct simulation of the turbulent flow in a channel, Jung *et al.* (1992) found that an induced oscillatory motion of a wall of the channel or the introduction of an oscillatory cross-flow resulted in significant attenuation of turbulence production and a persistent reduction in skin friction. It seems evident that these observed changes are related to the modification of the quasi-streamwise flow structures. We study the evolution of the coherent structures and their interaction with the surface beneath, when the latter is subjected to spanwise oscillation. Within the limitations of our model, we show that the interaction of the coherent vortex structures with the Stokes layer on the wall leads to a reduction in the skin friction, the Reynolds stress and the rate of production of fluctuating kinetic energy. The considerations illustrate how Orlandi–Jimenez type models can be used to study critical issues in boundary-layer control at a low computational cost. Similar studies were carried out by Choi, Moin & Kim (1994) for example.

2. Formulation and numerical method

We consider the flow in a Cartesian coordinate system $Ox^*y^*z^*$ with Ox^* along the streamwise direction so that $y^* - z^*$ is the cross-plane of interest (figure 1). The flow variables are non-dimensionalized with respect to the wall units. Thus $\boldsymbol{x}^* = (\nu^*/u_\tau^*)\boldsymbol{x}$,

$t^* = (\nu^*/u_\tau^{*2})t$, $\boldsymbol{u}^* = u_\tau^* \boldsymbol{u}$, $\boldsymbol{\omega}^* = (u_\tau^{*2}/\nu^*)\boldsymbol{\omega}$, $p^* = \rho^* u_\tau^{*2} p$, and so on, where $u_\tau^* = (\tau_w^*/\rho^*)^{1/2}$ is the friction velocity, τ_w^* is the shear stress at the wall, ρ^* is the fluid density and ν^* is the kinematic viscosity; the usual notation $\boldsymbol{x}^+ \equiv \boldsymbol{x}$ and $t^+ \equiv t$ is also used below without ambiguity.

As in Dhanak, Dowling & Si (1997), we consider the flow in the vicinity of the $x = 0$ plane, with the streamwise structure modelled by a two-dimensional vortex under-going axial stretching, distortion and translation in an imposed straining flow. The latter, represented by a Hiemenz flow, $(x\phi(y), -\phi(y), 0)$, approximately accounts for the flow induced by coherent structures in the outer flow field. The straining flow stretches vortex elements in the streamwise direction; according to (Schoppa & Hussain 1997), stretching plays an essential role in the generation of the coherent vortex structures. The function $\phi(y)$ is chosen here so that at large distances from the surface, the imposed flow is of the form, $(ax, -ay, 0)$, where a denotes the rate of axial strain associated with the outer flow. This choice of the imposed flow is based on the consideration of the flow field induced locally, in the vicinity of $x = 0$, by nearby three-dimensional coherent structures, for example, by the 'head' of a local hairpin-type structure. The velocity induced by such a structure acts to stretch the vortex elements aligned with the streamwise direction and drive them towards the wall (Dhanak & Dowling 1995). Alternatively, if the streamwise vortex is regarded as a misaligned attached eddy, then the straining flow may be considered to represent the effect of the misalignment.

The velocity field associated with a coherent streamwise vortex evolving under the imposed background flow is given by an exact solution of the Navier–Stokes equations, of the form,

$$\boldsymbol{u} = [q_0(y,z,t) + x(\phi'(y) + q_1(y,z,t)), -\phi(y) + v_1(y,z,t), w_1(y,z,t)], \tag{2.1}$$

where q_0, q_1, v_1 and w_1 satisfy equations described below, while $\phi(y)$ satisfies (Schlichting 1968):

$$\phi''' + \phi\phi'' - \phi'^2 + a^2 = 0; \quad \phi(0) = \phi'(0) = 0; \quad \phi'(y) \sim a \quad \text{as} \quad y \to \infty. \tag{2.2}$$

In view of (2.1), the vorticity $\omega(x,y,z,t)$ is given by

$$\left.\begin{aligned} &\boldsymbol{\omega}(x,y,z,t) = (\omega_{0x}, \omega_{0y} + x\omega_{1y}, \omega_{0z} + x\omega_{1z}); \\ &\omega_{0x} = \partial w_1/\partial y - \partial v_1/\partial z; \quad \omega_{0y} = \partial q_0/\partial z; \quad \omega_{1y} = \partial q_1/\partial z; \\ &\omega_{0z} = -\partial q_0/\partial y; \quad \omega_{1z} = -(\partial q_1/\partial y + \phi''). \end{aligned}\right\} \tag{2.3}$$

The streamwise component of vorticity ω_{0x}, satisfies

$$\left(\frac{\mathrm{D}}{\mathrm{D}t} - \nabla^2\right)\omega_{0x} = \omega_{0x}(q_1 + \phi'), \tag{2.4}$$

where

$$\nabla^2 = \frac{\partial^2}{\partial y^2} + \frac{\partial^2}{\partial z^2}, \quad \frac{\mathrm{D}}{\mathrm{D}t} = \frac{\partial}{\partial t} + (v_1 - \phi)\frac{\partial}{\partial y} + w_1\frac{\partial}{\partial z}.$$

As shown by Orlandi & Jimenez (1991), the equation for the streamwise contribution q_0 decouples from the other equations and does not influence the evolution in the cross-plane; it can be evaluated as a passive quantity once the cross-stream velocity components are determined. On substituting (2.1) into the momentum equations, we

obtain equations for q_0 and q_1,

$$\left(\frac{\mathrm{D}}{\mathrm{D}t} - \nabla^2\right) q_0 = -q_0(\phi' + q_1) - C_1, \tag{2.5}$$

$$\left(\frac{\mathrm{D}}{\mathrm{D}t} - \nabla^2\right) q_1 = -q_1(2\phi' + q_1) - v_1\phi'', \tag{2.6}$$

where the pressure gradient $\partial p/\partial x = C_1$, a constant, ensures that (2.1) is an exact solution of the equations of motion; C_1 is determined by initial conditions. We write

$$v_1 = \partial\psi/\partial z - \int_0^y q_1 \mathrm{d}y; \quad w_1 = -\partial\psi/\partial y. \tag{2.7}$$

If $q_1 \equiv 0$, then $\psi(y, z, t)$ represents the streamfunction (cf. Orlandi & Jimenez 1994). Using (2.4) and the continuity equation we obtain,

$$\nabla^2\psi = -\omega_{0x} + \int_0^y (\partial q_1/\partial z)\mathrm{d}y. \tag{2.8}$$

Equations (2.4) and (2.6–2.8), together with the appropriate boundary and initial conditions, suffice to determine the motion in the cross-plane, these equations being independent of q_0.

The contribution q_1 to the streamwise velocity, as well as cross-stream components v_1 and w_1, vanish as $y \to \infty$, so that away from the wall the influence of the coherent vortex is negligible and the velocity field is solely due to the outer background flow. Thus

$$\boldsymbol{u}(x, y, z, t) \sim (q_{00}(y) + x\phi', -\phi, 0) \quad \text{as} \quad y \to \infty,$$

where $q_{00}(y)$ is the streamwise velocity in the absence of the vortex and the straining flow. This condition is applied at the upper boundary of the computational domain, taken to be sufficiently far away, at $y = Y$. Further, the flow is considered to be periodic in the z-direction, with a wavelength Z. Thus, the boundary conditions for the velocity are taken to be:

$$\left.\begin{aligned} &\boldsymbol{u}(x, 0, z, t) = (0, 0, W_0 \cos[2\pi(t + \chi T)/T]); \quad \boldsymbol{u}(x, y, z + Z, t) = \boldsymbol{u}(x, y, z, t); \\ &\boldsymbol{u}(x, Y, z, t) = (q_{00}(Y) + x\phi'(Y), -\phi(Y), 0). \end{aligned}\right\} \tag{2.9}$$

Here T is the period of oscillation, W_0 is its amplitude and χ is a constant ($0 \leqslant \chi < 1$) which represents the phase of the oscillation at time $t = 0$ when the streamwise vortex structures are introduced in the flow.

The initial velocity distribution is taken to be

$$\boldsymbol{u}(x, y, z, 0) = (q_{00}(y) + x\phi'(y), -\phi(y), w_{00}(y, 0)). \tag{2.10}$$

In view of (2.5), $q_{00}(y)$ satisfies

$$q_{00}'' + \phi q_{00}' - \phi' q_{00} - C_1 = 0; \quad q_{00}(0) = 0; \quad q_{00}'(0) = 1, \tag{2.11}$$

where the constant C_1 is chosen to ensure that $q_{00}'(Y) = 1$. The latter condition implies that far away from the wall the streamwise velocity varies linearly. Other choices are possible; however, the exact choice is not critical to present considerations. The term q_{00} is shown as a solid line in figure 2(*a*). The spanwise component $w_{00}(y, t)$ is an exact solution of the Navier–Stokes equation, satisfying

$$\frac{\partial w_{00}}{\partial t} - \phi\frac{\partial w_{00}}{\partial y} - \frac{\partial^2\omega_{00}}{\partial y^2} = 0, \tag{2.12}$$

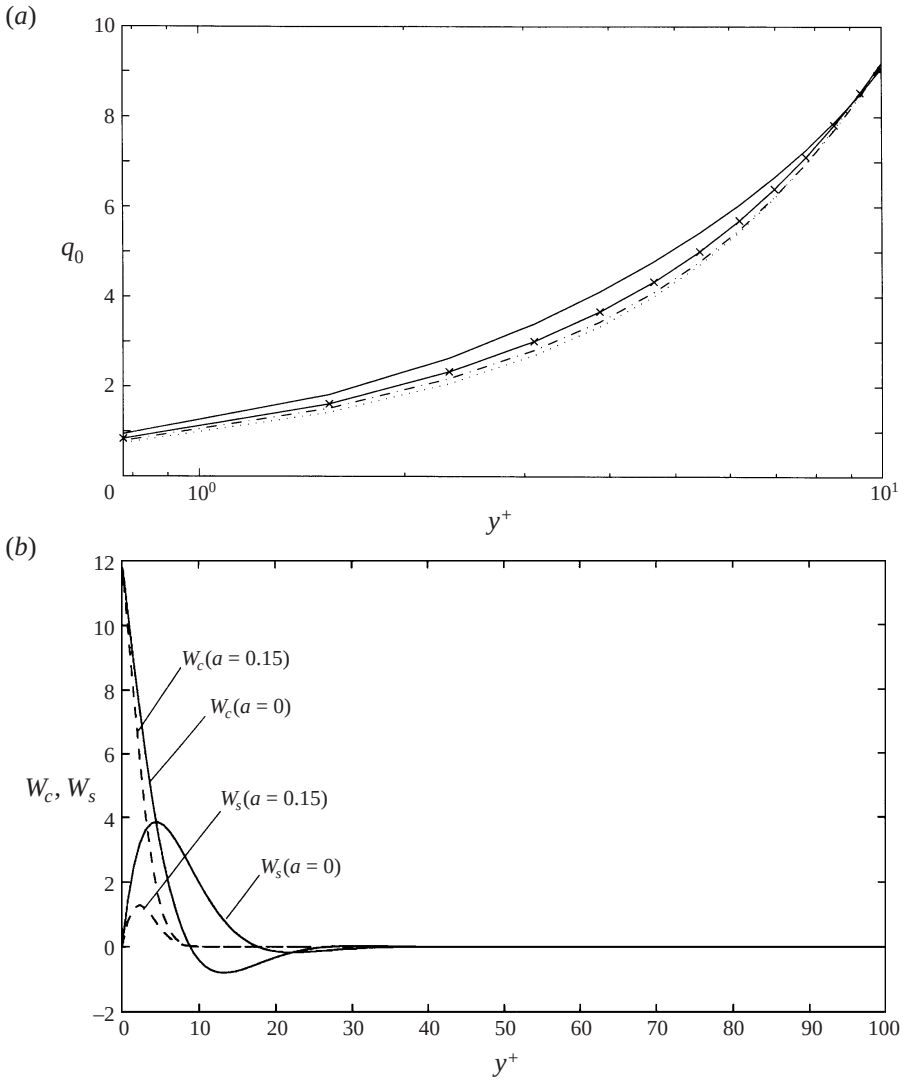

FIGURE 2. (*a*) Effect of spanwise oscillation, with $T = 100$, $W_0 = 12$, on mean streamwise velocity profile, averaged with respect to time and z, for the case $\Gamma = 300, a = 0.15$: ——, without oscillation; —·—·—, with oscillation, $\chi = \frac{1}{2}$; —×— with oscillation, averaged over phase χ. – – –, initial profile. (*b*) Amplitude functions W_c and W_s for the background oscillatory flow in the cross-plane in the presence of a straining flow with $a = 0.15$ is compared with corresponding functions associated with a Stokes layer ($a = 0$). Period $T = 100$, amplitude $W_0 = 12$.

together with the boundary condition (2.9) at the wall; the solution belongs to Lin's class of exact solutions and was first suggested by Wuest (1952, see Stuart 1963, p. 405). The term $w_{00}(y, t)$ represents the transverse velocity in a Stokes layer in the presence of axial stretching and is given by

$$w_{00} = W_c(y, T)\cos[2\pi(t/T + \chi)] + W_s(y, T)\sin[2\pi(t/T + \chi)], \tag{2.13}$$

where W_s and W_c satisfy appropriate ordinary differential equations. In the absence

of the straining flow (i.e. $\phi(y) \equiv 0$), W_s and W_c are, respectively, given by (Schlichting, p. 85):

$$W_c = W_0 e^{(-\pi/T)^{1/2}y} \cos[(\pi/T)^{1/2}y]; \quad W_s = W_0 e^{-(\pi/T)^{1/2}y} \sin[(\pi/T)^{1/2}y], \tag{2.14}$$

where W_0 is a constant. The thickness of the layer, in this case, increases with the increase in the period of oscillation, so that we expect the intensity of the interaction between the coherent structures and the Stokes layer to increase with the increase in period of oscillation, at least for small enough periods. For larger periods, the magnitude of the vorticity, for a fixed y, becomes the case smaller according to $\sim 1/T^{1/2}$ and we accordingly expect the effect to diminish. When a plane straining flow is present, the layer characteristics are modified as illustrated in figure 2(b) for a particular value of T. Most significantly, the layer thickness is reduced.

We determine w_{00} from (2.13) for various values of χ, each case corresponding to the phase of the oscillation relative to the time of appearance of the coherent vortices in the wall region. The wall statistics are then determined from averaging over the different phases.

The initial vorticity distribution can be written in the form

$$\boldsymbol{\omega}(x, y, z, 0) = \left(\omega_{x00}(y, z) + \frac{\partial w_{00}}{\partial y}, 0, -q'_{00} - x\phi''\right) \tag{2.15}$$

where the streamwise component $\omega_{x00}(y, z)$ is to be appropriately prescribed. Here, we consider ω_{x00} to be that given by Orlandi & Jimenez (1994), where the coherent vortices develop from vortex sheets in the buffer region, although other appropriate distributions may be considered. Thus

$$\boldsymbol{\omega}_{x00}(y, z) = \frac{\Gamma h \pi^{1/2}}{2S} \exp\left(-\frac{n^2}{h^2}\right) \sin(\pi s/S), \tag{2.16}$$

where $s = (\boldsymbol{x} - \boldsymbol{x}_1) \cdot \hat{\boldsymbol{s}}, \boldsymbol{n} = (\boldsymbol{x} - \boldsymbol{x}_1) \cdot (\boldsymbol{i} \times \hat{\boldsymbol{s}})$ with $\hat{\boldsymbol{s}} = (\boldsymbol{x}_2 - \boldsymbol{x}_1)/S$ and $S = |\boldsymbol{x}_2 - \boldsymbol{x}_1|$. $h = 0.75$ and $\boldsymbol{x}_1 = (0, 15, 10)$ and $\boldsymbol{x}_2 = (0, 10, 50)$ for the first vortex sheet and $\boldsymbol{x}_1 = (0, 10, 50)$ and $\boldsymbol{x}_2 = (0, 5, 60)$ for the second sheet. An alternative introduction of the vortices is considered in Dhanak *et al.* (1997). The present model is based on the assumption that whereas the formation of the coherent structures involve complex three-dimensional processes, details of which are not considered here, the surface skin friction is principally governed by the subsequent interaction of the quasi-streamwise structures with the rigid surface.

The numerical method of solution is similar to that described by Orlandi & Jimenez (1994). Thus, the problem is solved in the rectangular domain $0 \leqslant z \leqslant Z, 0 \leqslant y \leqslant Y$ with periodic boundary conditions at $z = 0$ and $z = Z$. In the results presented here, $Y = Z = 100$ was chosen; this is consistent with the minimal flow unit proposed by Jimenez & Moin (1991). Equations (2.4)–(2.7) are solved in a time marching scheme with the viscous and the nonlinear terms discretized by centred differences. Time advancement is via a third-order Runge–Kutta method with two-level storage, explicit for the nonlinear terms and implicit for the viscous terms. For each subtimestep, the velocity information is updated by solving two tridiagonal matrices using an alternating direction implicit (ADI) method for the implicit viscous terms. The vorticity boundary condition used is second-order accurate in time and space, consistent with the accuracy of the difference equations. Poisson equation (2.8) for ψ together with boundary conditions (2.9), is solved using fast Fourier transforms in the z-direction and tridiagonal solvers in the y-direction. The numerical code was

checked by reproducing, to good agreement, the results of Orlandi & Jimenez (1994). Results presented here are for a 128×128, equally spaced, rectangular grid. The adequacy of this was verified through comparison with computations with 64×64 and 256×256 grids; for a measure of the computational error in the calculation, please see Dhanak *et al.* (1997). Evolution of the vortices was considered over a time $T_f = 40$, with a timestep $\Delta t = \frac{40}{1024}$.

The exact solution described above may be extended to consider a general outer flow, approximately valid in the vicinity of $x = 0$, by expanding the latter as well as other flow quantities in terms of a Taylor series in x (cf. equation (2.1)), substituting the expressions in the Navier–Stokes equations and approximately solving the resulting set of equations of the type (2.5)–(2.6).

3. Results

The parameters of the problem are the initial total circulation around each vortex or vortex strength Γ, the strain rate a, the initial streamwise vorticity distribution, the oscillation period T, the amplitude W_0 and the phase χ. $\Gamma \equiv \Gamma^+$ also denotes the vortex Reynolds number of the flow. Robinson (1991) gives statistics of the strength, height and size of coherent streamwise circular vortex structures observed in a numerical simulation of boundary-layer flow at a particular Reynolds number. Typically, $\Gamma^+ \sim 50 - 500$, and the vortices are observed in the buffer region at heights $\sim 10 - 20$ wall units, and have radii $R^+ \sim 5 - 20$. Further, Orlandi & Jimenez (1991) estimate that the axial strain rate $a^+ \sim 0.1 - 0.3$. For the purpose of examining the effect of spanwise oscillation, we consider the initial form of the coherent structures to be in the form of sheets given by (2.16), as in Orlandi & Jimenez (1994), but with the strength and strain rate given by $\Gamma^+ = \pm 300$ and $a^+ = 0.15$; this distribution quickly evolves into what may be considered as fairly representative, although the strength of the vortices need not be equal and opposite. Similar results to those presented here may be obtained using single vortices instead of the pair. The effect of varying Γ and a is examined later.

The effect of the oscillation on the evolution of the chosen initial distribution was considered for a range of values of T and χ for a fixed value of $W_0^+ = 12$, this value being chosen so that it corresponds to that considered by Jung *et al.* (1992) in their DNS study. A number of cases corresponding to a range of values of the period T were computed. The streamwise velocity profile averaged over the spanwise (z) domain and over time t for the particular case in which the wall oscillates with period $T^+ = 100$ is compared in figure 2(a) with the corresponding profile in the absence of the oscillation and with the intital profile. The profiles may be compared with the mean profiles in the DNS study of Jung *et al.* and with the mean profiles measured in experiments (Laadhari, Skandaji & Morel 1994). The effect of the oscillation is to reduce the mean streamwise velocity gradient.

The development of the vorticity distribution in the cross-plane with respect to time is illustrated in figure 3 where streamwise vorticity contours are depicted; the convention used is that positive values of ω_{0x} imply clockwise rotation. Figure 3(a) depicts the case in the absence of wall oscillation. The vortex sheets roll-up in time $t^+ = O(1)$. The interaction between each vortex structure and the wall beneath results in the development of a layer of vorticity of opposite sign to that of the vortex on the wall. As pointed out by Orlandi & Jimenez (1991), the straining flow induces a movement of the vortex towards the wall and the subsequent interaction results in ejection of the vorticity in this layer away from the wall. As the distance

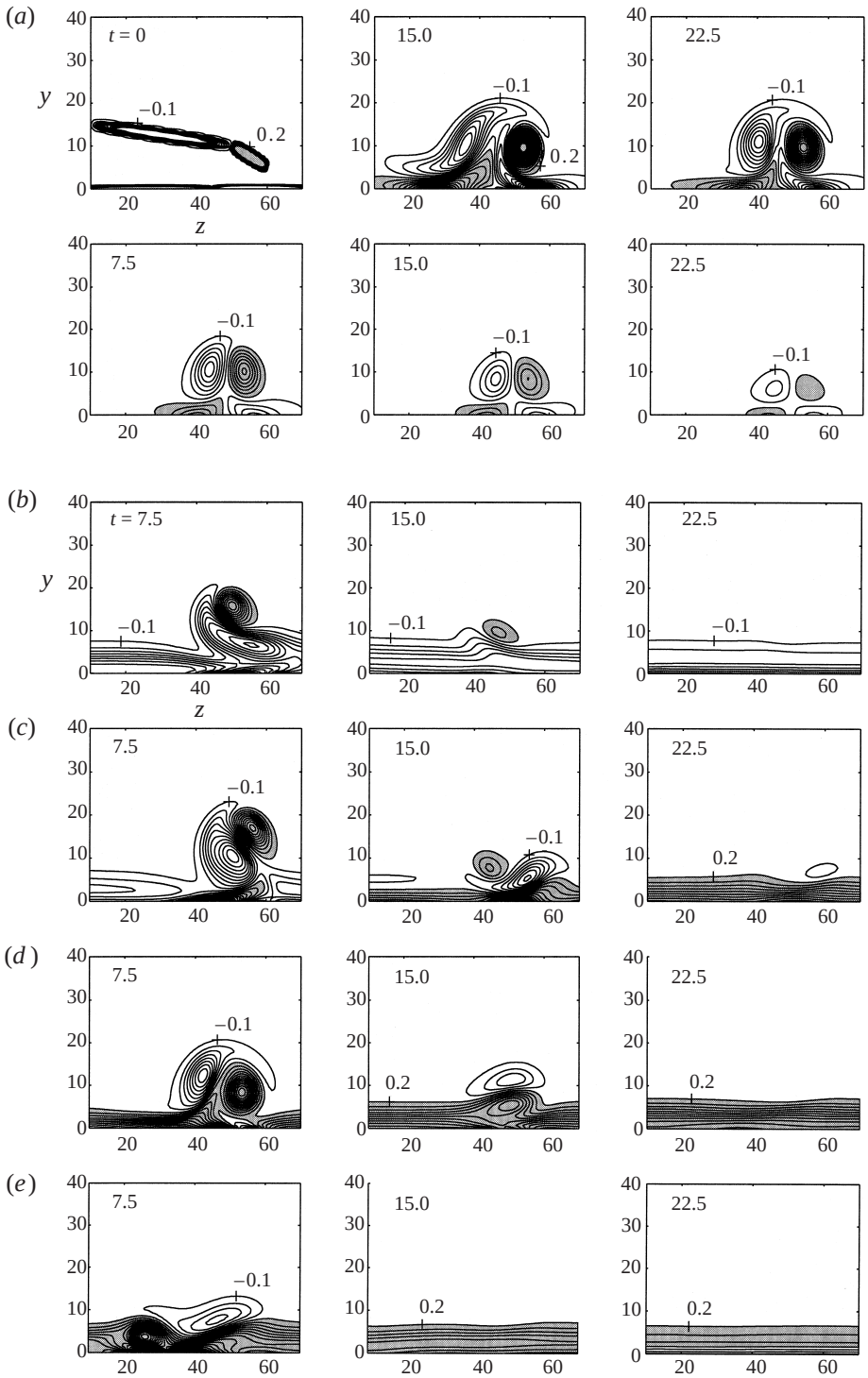

FIGURE 3. For caption see facing page.

separating the vortices gets smaller, the self-induced velocity of the pair tends to move away from the surface, but this motion is opposed by the straining flow and the vortices undergo a mutual, viscous annihilation at a finite distance from the wall. The evolution was followed for time $t^+ = 40$, at which time the coherent vortices, though still distinguishable, are very weak. Orlandi & Jimenez, on the basis of dimensional analysis, however, argue that the quasi two-dimensional interaction in the cross-plane can strictly be regarded as representative of flow associated with coherent structures in the near-wall region of a turbulent boundary layer for times $t^+ = O(20)$; for subsequent times the three-dimensional effects neglected in the model become important and need to be accounted for. In figure 4(*a*), we show the instantaneous streamwise velocity contours in the cross-plane corresponding to the evolution shown in figure 3(*a*). As pointed out by Orlandi & Jimenez, these feature a central region of low-speed fluid which is ejected away from the surface, flanked by regions of high-speed fluid which are swept towards the surface, forming a characteristic low-speed streak. The corressponding instantaneous distributions of $u'v'$, representing local contribution to Reynolds stress are shown in figure 5(*a*). The figure clearly shows the dominance of the region over which $-u'v'$ is positive, implying an increase in Reynolds stress and the rate of production of turbulent energy.

For a given period and amplitude of spanwise wall oscillation, the influence of the oscillation on the interaction depends on its phase χ relative to the time of introduction of the streamwise vortices. Figure 3(*b–e*) illustrates the contours of evolving vorticity, corresponding to those shown in figure 3(*a*), in cases where the wall performs spanwise oscillations with period $T^+ = 100$ and amplitude $W_0^+ = 12$ for a range of values of χ. The modified Stokes layer (see figure 2*b*) is fairly thin. However, depending on the value of χ, it not only affects the viscous response at the surface, but also significantly influences the evolution of the vortex pair. For the cases shown in figure 3(*b*) and 3(*c*) ($\chi = 0, \frac{1}{8}$ respectively), the wall moves to the right over the lifetime of the eddy and the modified Stokes layer is well established when the vortices are introduced. In the ensuing interaction, the left vortex gets swept underneath the right vortex and undergoes rapid viscous annihilation. By around $t^+ = 20$, neither of the coherent structures are visible, in contrast to the case in the absence of oscillation (figure 3*a*) when the structures are still distinguishable at $t^+ = 40$. The structure of the wall response layer is also significantly different. Further, the relative orientation of the vortices during the evolution implies a significantly less efficient transfer of vertical momentum than in the case without oscillation. The associated effects on the streamwise velocity and local contribution to Reynolds stress are shown in figures 4(*b, c*) and 5(*b, c*), respectively. By around $t^+ = 4$, the development of the low-speed streak is signficantly different and vanishes rapidly by around $t^+ = 20$. The oscillations induce mixing of high-speed and low-speed fluid close to the wall. The corresponding change in the distribution of $u'v'$ can be seen from figure 5(*b*) and 5(*c*); the regions of positive contribution to Reynolds stress ($-u'v'$) are significantly reduced and subsequently vanish much earlier than in the absence of oscillation.

FIGURE 3. (*a*) Evolution of streamwise vorticity in the absence of oscillation. $\Gamma = 300$, $a = 0.15$. (*b*)–(*e*) Evolution of streamwise vorticity for spanwise oscillation of the surface $y = 0$, with period $T = 100$ and amplitude $W_0 = 12$ and with $\Gamma = 300$, $a = 0.15$: (*b*) $\chi = 0$; (*c*) $\chi = \frac{1}{8}$; (*d*) $\chi = \frac{1}{4}$; (*e*) $\chi = \frac{1}{2}$. In each case, vorticity contours in (y, z) cross-plane are shown at various times. $\Delta\omega_x = 0.3$, shaded contours denoting positive ω_x.

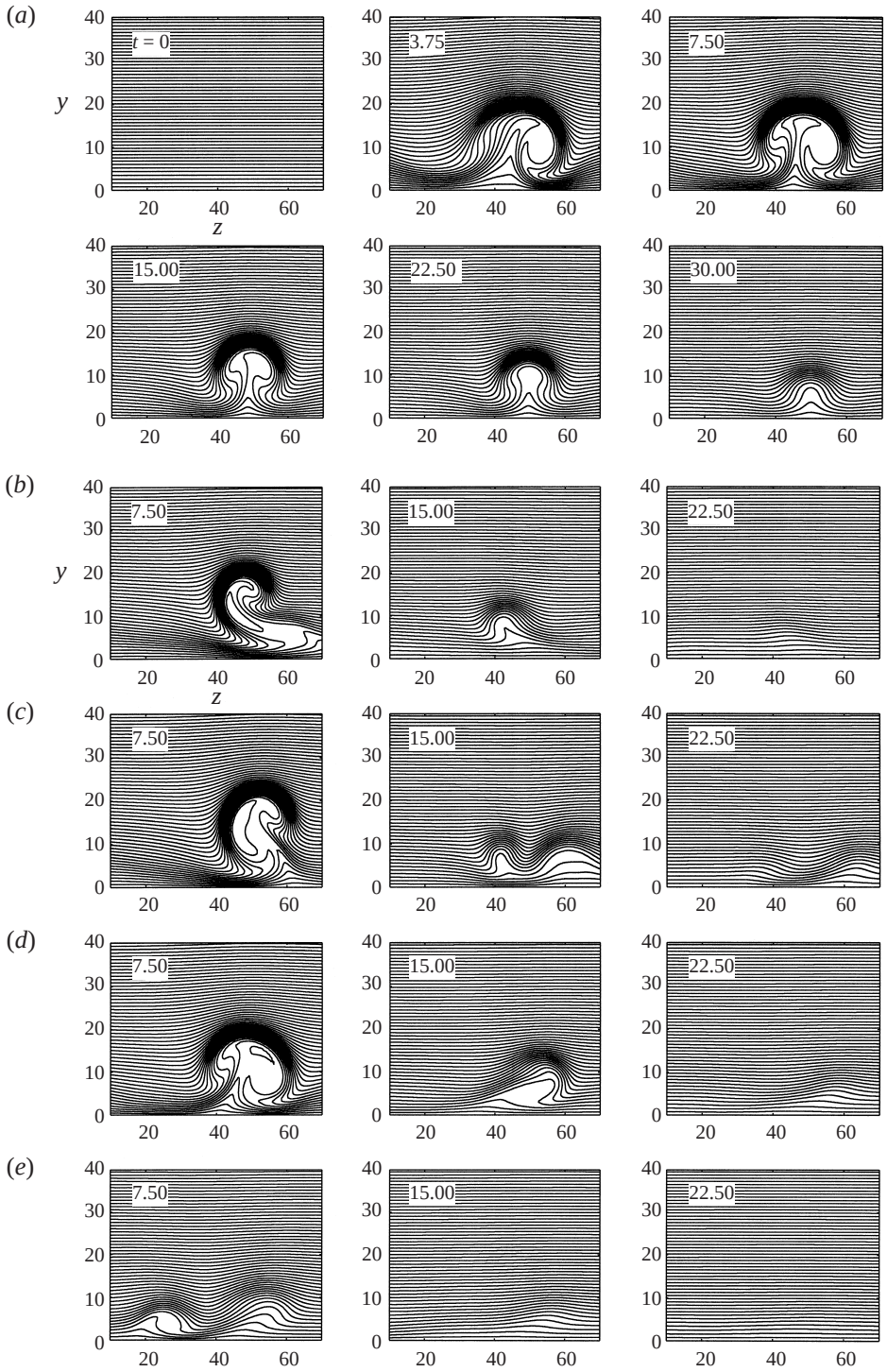

FIGURE 4. For caption see facing page.

For $\chi = \frac{1}{4}$, we see from (2.13) that at $t = 0$, the modified Stokes layer is rather weak and the wall begins to move from right to left. As a result the influence of the oscillation on the interaction is relatively slower, with the structures maintaining their status fairly well (figure 3*d*) until around $t^+ = 10$ when the right vortex is swept underneath the left vortex. Consequently, the vortices undergo rapid viscous annihilation as before. The associated delayed annihilation of the low-speed streak and the regions of positive contributions to the Reynolds stress ($-u'v'$) can be seen from figures 4(*d*) and 5(*d*), respectively.

For $\chi = \frac{1}{2}$ the oscillation has a maximum impact on the coherent vortex pair (figure 3*e*). The modified Stokes layer is again well established at $t = 0$, with the wall surface moving from right to left and induces the right vortex to move beneath the left vortex, thereby inducing, once again, a rapid annihilation of the coherent structures and significant mixing of low-speed and high-speed fluid (figure 4*e*) and a significant reduction in the region over which ($-u'v'$) is positive (figure 5*e*). By around $t^+ = 10$, the coherent structures have almost vanished.

Figure 6(*a*) shows the effect of the oscillation on the growth of skin friction with time for the particular case in which the period of oscillation is $T^+ = 100$. The average, $\overline{\tau_w} = \overline{\partial q_0/\partial y}|_{y=0}$, over z is shown plotted as a function of time. In the absence of the oscillation, Orlandi & Jimenez (1994) had shown that for small times with $a^+ = 0$, the skin friction increases with time. We see from figure 6(*a*) that this is true also for non-zero values of a and that for larger times as the viscous pair undergo viscous annihilation, the skin friction reduces to its original value of 1, the relaxation time being around $t^+ = 40$. When the wall oscillates, the maximum value of the skin friction and the relaxation time are both reduced, the value of the reduction depending on the phase χ; the maximum reduction corresponds to $\chi = \frac{1}{2}$.

Assuming that it is equally likely that the coherent structures are generated in a particular phase, we average over these phases. In figure 6(*b*), this average value, denoted $\overline{\tau_w^{(osc)_m}}(t^+)$, is compared with the corresponding value, $\overline{\tau_w^{(0)}}(t^+)$, in the case without oscillation. For the case $T^+ = 100$ depicted, the maximum value of $\overline{\tau_w}^{(osc)_m}$ is 10% smaller and the relaxation time 42% shorter than for $\overline{\tau_w^{(0)}}$.

In figure 7, we examine the influence of the oscillation period T on the results. The time evolution of the ratio $Q(t^+) = \overline{\tau_w^{(osc)_m}}/\overline{\tau_w^{(0)}}$ between the mean (with respect to z and the phases χ) skin friction in the presence of the oscillation to that in the absence of it, is shown in figure 7(*a*). Although it is not possible to make a direct comparison with the results of Jung *et al.*'s (1992) DNS study, this figure is consistent with their figure 1 for $t^+ < 20$. We see from figure 7(*a*) that for $t^+ > 3$, Q decreases with time from its value of around 1. The reduction is weakly dependent on period for these small times, though at around $t^+ = 20$, it is clear that, of the cases considered, Q is minimum for $T^+ = 75$ and maximum for $T^+ = 500$. For $t^+ > 20$, the influence of three-dimensional effects become important and the present quasi two-dimensional model is no longer adequate. Further, the influence of larger-scale structures in the outer region of the boundary layer, not included in the present model, will become significant. In their DNS simulation, Jung *et al.* found that for $t^+ > 50$ the ratio

FIGURE 4. (*a*) Evolution of streamwise velocity in the absence of oscillation. $\Gamma = 300, a = 0.15$. (*b*)–(*e*) Evolution of streamwise velocity for spanwise oscillation of the surface $y = 0$. with period $T = 100$ and amplitude $W_0 = 12$ and with $\Gamma = 300$, $a = 0.15$: (*b*) $\chi = 0$; (*c*) $\chi = \frac{1}{8}$; (*d*) $\chi = \frac{1}{4}$; (*e*) $\chi = \frac{1}{2}$. In each case, streamwise velocity contours in (y, z) cross-plane are shown at various times. $\Delta q_0 = 0.75$.

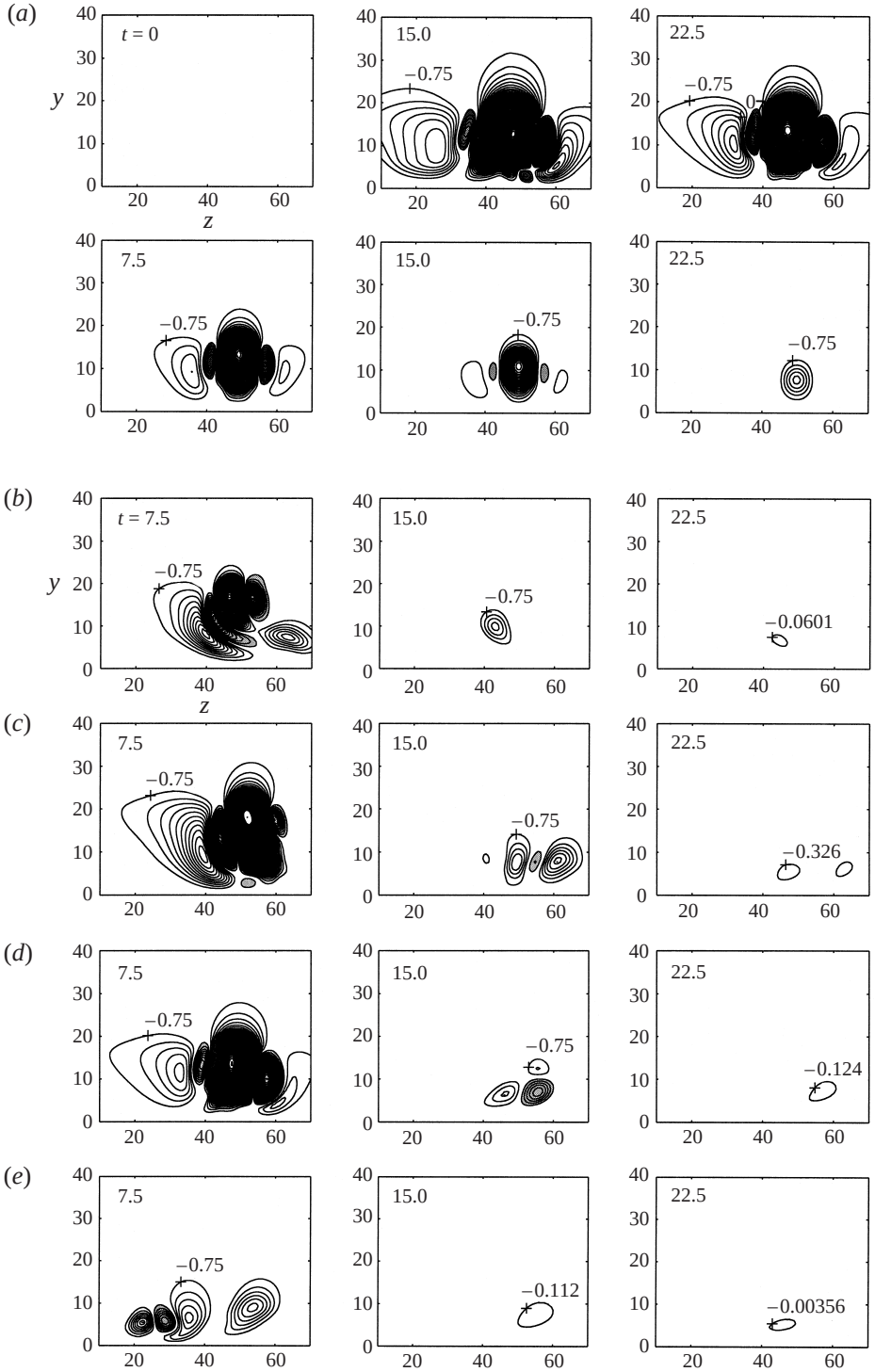

FIGURE 5. For caption see facing page.

of the mean skin friction in the presence of oscillation to that in the absence of it becomes very much dependent on the period T. They found that the value of this ratio at around $t^+ = 500$ was approximately 0.95 for $T^+ = 25$, 0.6 for $T^+ = 100$ and 0.9 for $T^+ = 200$; for $T^+ = 500$, the ratio oscillated in time between the values 1 and 1.3 over the range $50 < t^+ < 500$. Such large-time behaviour is beyond the scope of the present model.

The ratio $t_R^{(osc)}/t_R^{(0)}$ between the relaxation time in the presence of oscillation to that in the absence of it is plotted against the period T in figure 7(*b*). The ratio decreases from a value of approximately 0.65 for $T^+ = 25$ to a minimum value of 0.57 approximately for $T^+ = 75$ and then increases to around 0.75 for $T^+ = 500$. The ratio

$$C_f^{(osc)}/C_f^{(0)} = \overline{\overline{\tau_w^{(osc)_m}}}/\overline{\overline{\tau_w^{(0)}}},$$

where the two bars denote averages over $t(0 < t^+ < 40)$ and z and m indicates an average over χ, is shown in figure 7(*c*). The figure suggests an overall reduction of around 10% in skin friction for all T over the time interval considered.

In the present model, we considered $\Gamma^+ = \pm 300$ and $a^+ = 0.15$. However, in a turbulent boundary layer, a range of vortex strengths are possible and the local strain rate, which is induced by larger eddies in the outer layer, can vary. In figure 8, we show how the effect of the oscillation on $C_f^{(osc)}/C_f^{(0)}$, depends on χ, a and Γ for a fixed value of period $T^+ = 100$. With a and Γ fixed also, the ratio oscillates (figure 8*a*) between 0.95 and 0.85 over the range of χ, the minimum corresponding to $\chi = \frac{1}{2}$. For fixed $\Gamma^+ = \pm 300$, the variation of $C_f^{(osc)_m}/C_f^{(0)}$, where the subscript m indicates an average over χ, with a over the range $0.1 < a^+ < 0.2$ is shown in figure 8(*b*). The plot indicates that somewhat better reduction may be obtained for a smaller value of a than used here. However, if a is reduced much further, the coherent structures tend to move away from the surface as they approach each other, so that the relaxation times will be rather long. The variation of $C_f^{(osc)_m}/C_f^{(0)}$ with Γ for a fixed value of $a^+ = 0.15$ is shown in figure 8(*c*). The plot suggests that smaller reductions in skin friction would be obtained with weaker vortices.

Figure 9(*a*) shows the effect of the oscillation on the average Reynolds stress distribution associated with the interaction. The distribution of $-\overline{u'v'}$ in the absence of the oscillation, denoted with a superscript (0) in the figure, shows characteristic behaviour for turbulent boundary layers, increasing to a maximum value in the region of the buffer layer, around $y^+ \simeq 13$, and vanishing away from the wall. In a turbulent boundary layer, the actual magnitude of the contribution to $-\overline{u'v'}$ at each y^+ from interactions of the type considered here depends on the number density of the distribution of coherent structures of different vortex strengths, in the range $50 \leqslant \Gamma^+ \leqslant 500$, and, at any instant, at various stages of decay (cf. Pullin & Saffman 1998). The wall oscillations produce a significant reduction in the magnitude of the Reynolds stress, the extent of the reduction being dependent on the phase χ. The maximum reduction is obtained for $\chi = \frac{1}{2}$. If we consider all phases to be equally likely and average the results over χ, then the result is as illustrated in figure 9(*b*).

FIGURE 5. (*a*) Evolution of Reynolds stress in the absence of oscillation. $\Gamma = 300$, $a = 0.15$. (*b*)–(*e*) Evolution of Reynolds stress for spanwise oscillation of the surface $y = 0$, with period $T = 100$ and amplitude $W_0 = 12$ and with $\Gamma = 300$, $a = 0.15$: (*b*) $\chi = 0$; (*c*) $\chi = \frac{1}{8}$; (*d*) $\chi = \frac{1}{4}$; (*e*) $\chi = \frac{1}{2}$. In each case, contours of $u'v'$ in (y, z) cross-plane are shown at various times. $\Delta u'v' = 0.75$, shaded contours denoting positive values of $u'v'$.

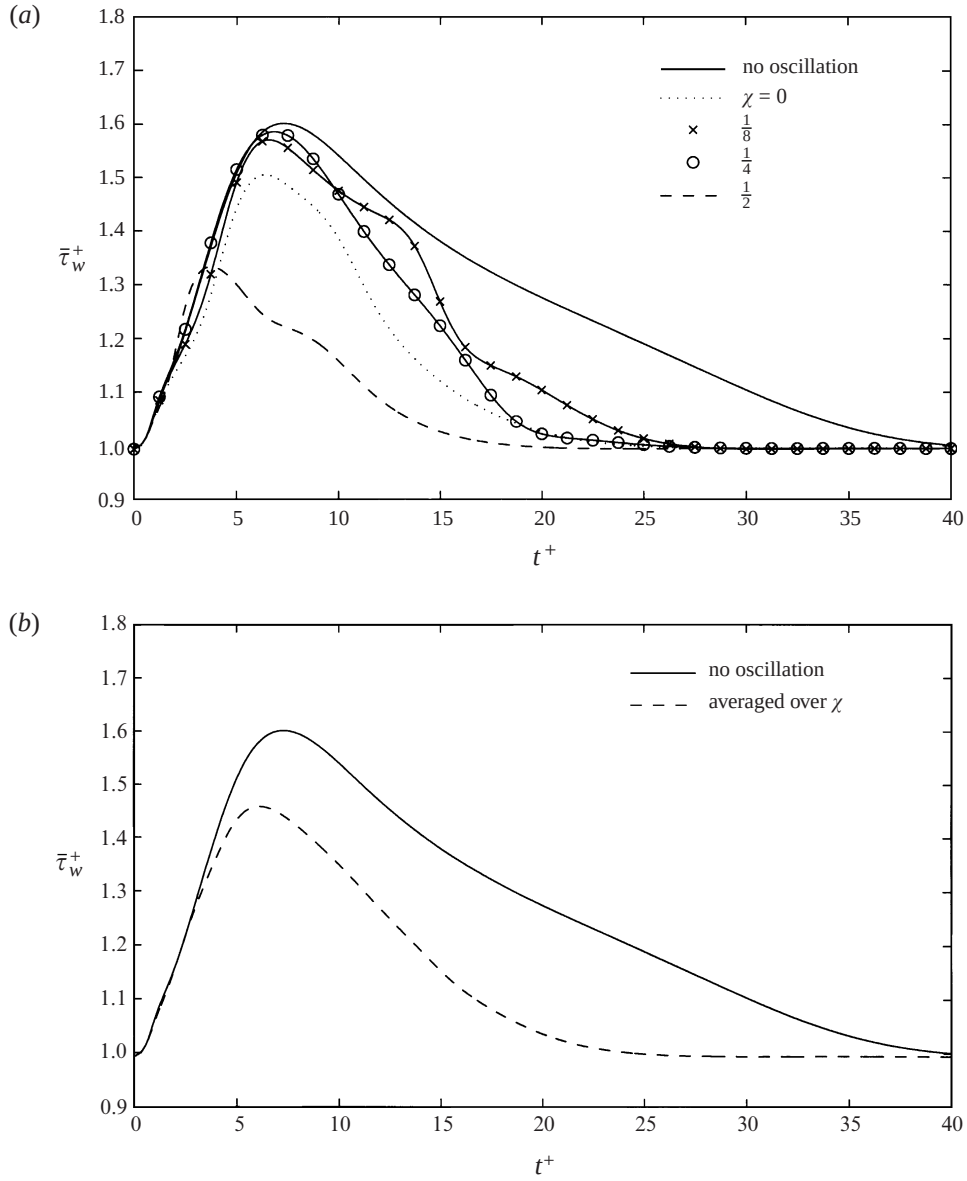

FIGURE 6. (*a*) Effect of spanwise oscillation on time evolution of the skin-friction for $\Gamma = 300, a = 0.15$. The skin friction in the absence of oscillation is compared with that in the presence of spanwise wall oscillation with $T = 100$, $W_0 = 12$ for different phases χ. (*b*) As in (*a*), but showing the comparison of the time evolution of the skin friction in the absence of oscillation with the corresponding skin friction, averaged over eight equally spaced phases χ, in the oscillatory case.

The maximum value of this average value, denoted $-\overline{u'v'}^{(osc)_m}$, is approximately half that for the case without oscillation; the maximum occurs at $y^+ \simeq 13$ in the absence of oscillation and at $y^+ \simeq 14$ in the presence of oscillation.

The corresponding rate of production of fluctuating kinetic energy associated with the interaction may be estimated from the term $-\overline{u'v'}(\overline{\mathrm{d}q_0/\mathrm{d}y})$ in the energy equation.

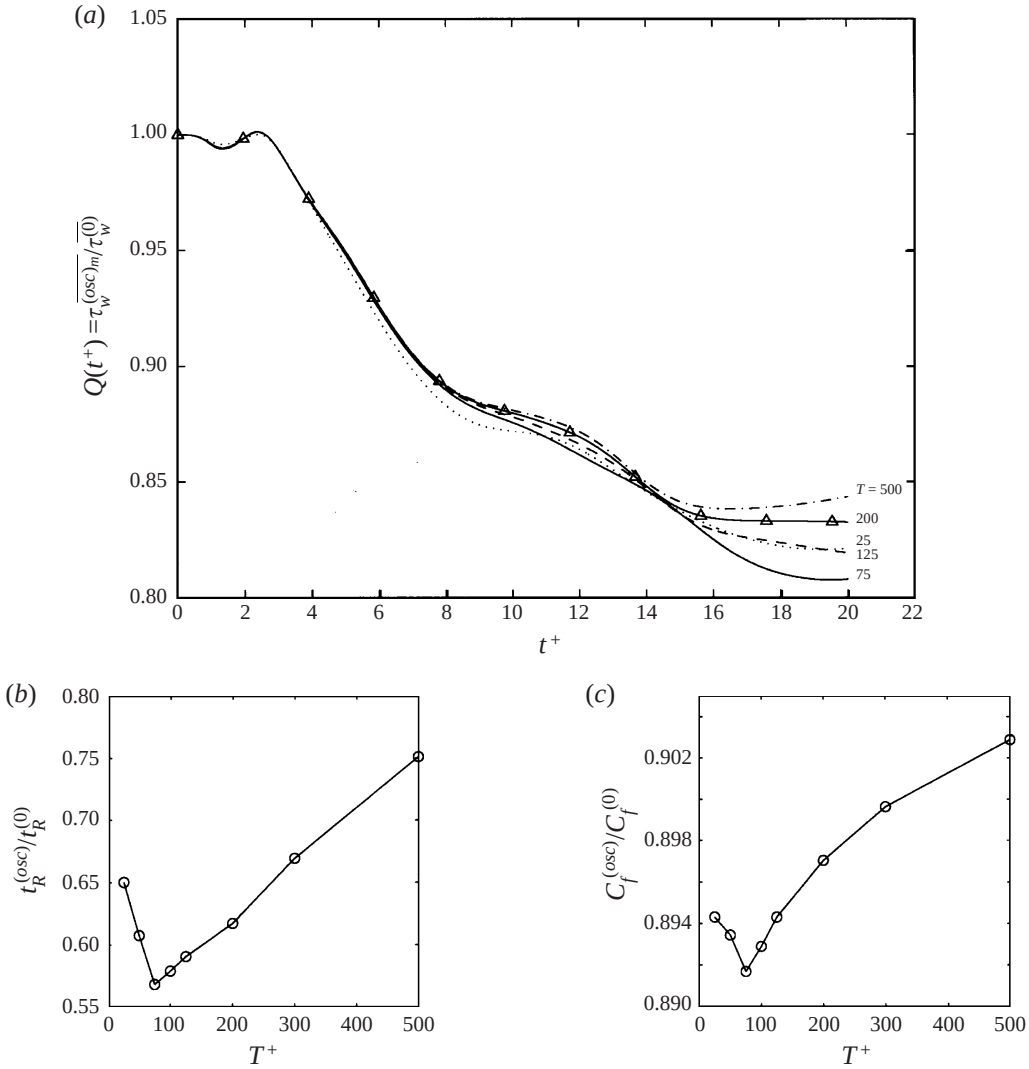

FIGURE 7. (*a*) Evolution of the ratio, $Q(t^+)$, of the skin-friction in the oscillatory case, averaged over z and phase χ, to the corresponding value in the absence of oscillation for various values of the period T. $\Gamma^+ = 300$, $a^+ = 0.15$, $W_0^+ = 12$. (*b*) Ratio of relaxation times $t_R^{(osc)}$ and $t_R^{(0)}$ as a function of oscillation period T. (*c*) Ratio of averaged (with respect to z, t and χ) skin friction, $C_f^{(osc)}$ and $C_f^{(0)}$ as a function of oscillation period T.

$-\overline{u'v'}(\overline{\mathrm{d}q_0/\mathrm{d}y})$ is plotted against y in figure 10. In the absence of oscillation, the predicted distribution of this rate may be compared with that given for the wall region of a pipe flow by Hinze (1975, p. 736); the shape of the curve and the location of the peak are in qualitative agreement, however, the magnitudes of the peak values differ since in turbulent flow this would depend not only on the number density of coherent structures of the type considered here but also on the magnitudes of their different strengths and, at any instant, on the stage of their decay. It is clear, however, that oscillatory motion produces a significant reduction in this rate, consistent with the observations in the DNS calculation (Jung *et al.* 1992). The maximum reduction

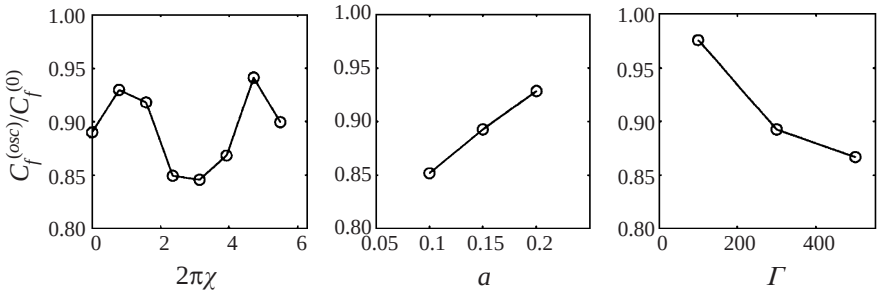

FIGURE 8. Variation of $C_f^{(osc)}/C_f^{(0)}$ with (a) phase χ for fixed $a = 0.15$, $\Gamma = 300$; (b) with strain rate a for fixed $\Gamma = 300$ and averaged over χ; (c) with vortex strength Γ for fixed $a = 0.15$ and averaged over χ. $T = 100$, $W_0 = 12$ in each case.

again occurs for $\chi = \frac{1}{2}$ (figure 10a) and the maximum value of the average rate of production (figure 10b) in the presence of wall oscillation is approximately half that for the case without oscillation.

In order to check the influence of the chosen initial conditions (2.10) and to assess if averaging over the phases χ is justified, we computed the cases shown in figure 3(a) and 3(b) over a long time, up to $t^+ = 400$, introducing new, identical structures at an interval of $t^+ = 40$. By introducing the vortices periodically in the manner described, so that a vortex introduced earlier has not completely died away before a next one is introduced, we can set up, over several cycles, conditions such that when the final vortex is introduced, the pre-existing conditions are very different from (2.10). The development of the skin friction $\overline{\tau}_w$ is shown in figure 11. The structure–wall interactions, and ensuing introduction of the final vortex, did not significantly differ from the one corresponding to the chosen initial conditions (2.10). Please note that the constraint on the validity of the model still corresponds to $t^+ < O(20)$, where $t^+ = 0$ corresponds to the time of introduction of the final vortex. Further, averaging over the duration of the computation gave results fairly similar to those, described above, obtained by averaging over χ, suggesting that the approach considered here is reasonable.

Finally, in figure 12 we show the influence of the oscillation on the contribution, $f(q_1/q_{1rms})$, of a single localized vortex pair to the probability density function for $\partial u'/\partial x = q_1$ associated with the cases depicted in figure 3; according to Schoppa & Hussain (1997), vortex stretching associated with positive values of $\partial u'/\partial x$ is of some importance in the process by which the coherent vortices are generated. The p.d.f. of $\partial u/\partial x$ is typically measured in experiments involving turbulent flow and has a characteristic shape whose deviation from a Gaussian is usually attributed to intermittent and localized occurrence of coherent structures of the type considered here; the p.d.f. has a shape in the form of a stretched exponential with significantly higher values at the tails (see for example, Frisch 1995). It is emphasized that in a turbulent boundary layer, unlike in figure 12, the p.d.f. is associated with a distribution of various coherent structures of different strengths and at different stages in their evolution (cf. Dhanak *et al.* 1997). However, it is interesting to note that the contribution to such a p.d.f. from a single vortex pair, shown in figure 12, has a distinct 'stretched exponential' appearance and see how such contributions could help render the shape of the p.d.f. of $\partial u'/\partial x$ in a turbulent boundary layer characteristically non-Gaussian. The values of $f(\eta_j)$ at discrete values η_j were determined by counting values of q_1, over the entire space–time simulation domain, which fall within a suitably sized bin $\Delta\eta_j$ centred around η_j; for the oscillatory case, $f(q_1/q_{1rms})^{(osc)}$ for individual

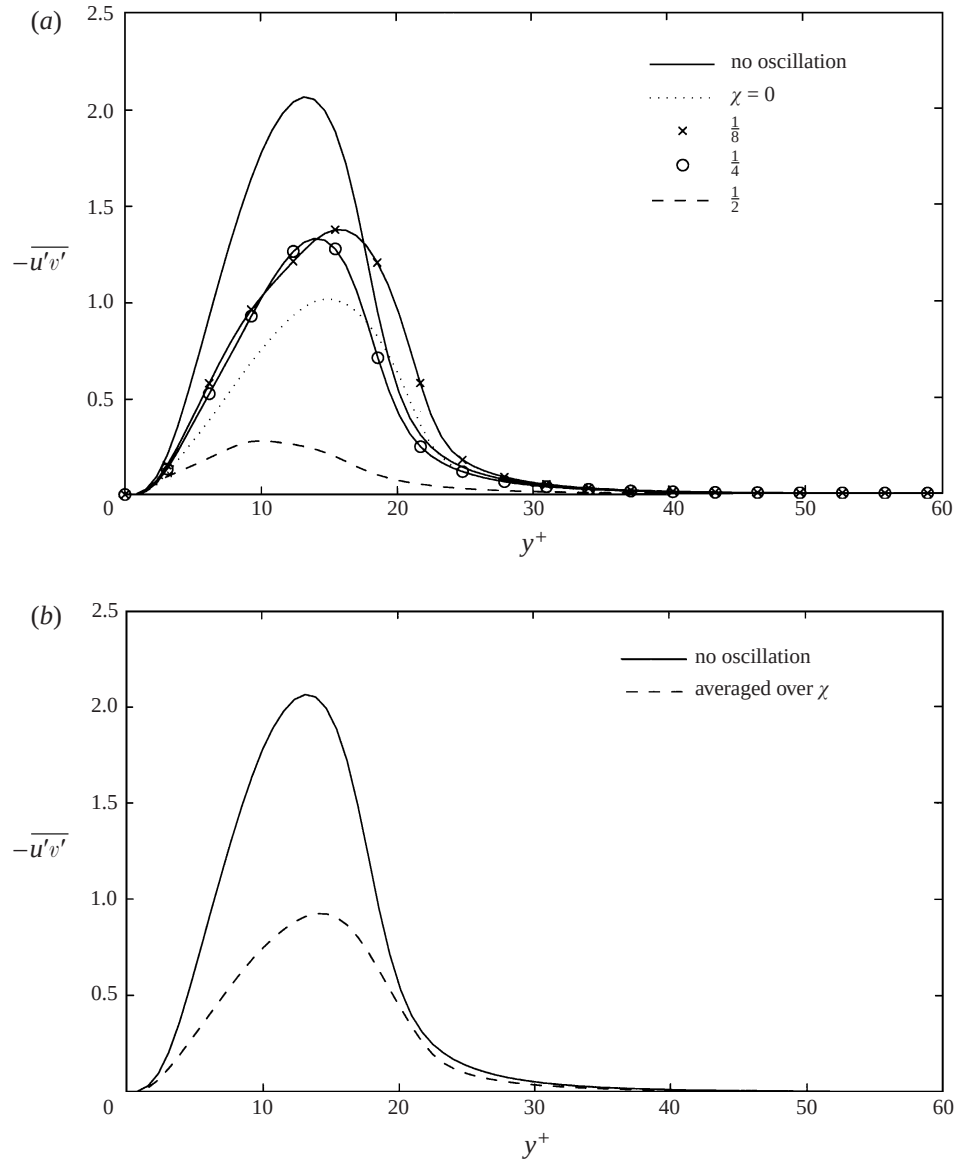

FIGURE 9. (*a*) Effect of spanwise oscillation on Reynolds stress. The Reynolds stress in the case without oscillation is compared with that for the oscillatory ($T = 100$, $W_0 = 12$) case for different values of the phase χ. The bar denotes average over z and t. $\Gamma = 300$, $a = 0.15$. (*b*) As in (*a*), but showing the comparison of the Reynolds stress in the absence of oscillation with the corresponding stress, averaged over eight equally spaced phases χ, in the oscillatory case.

phases were averaged over the phases. The normalized Gaussian distribution is included in the plot for comparison. The differences between $f^{(osc)}$ in the oscillatory case (dashed curve) and $f^{(0)}$ in the non-oscillatory case (solid curve) is not readily apparent for small values of $|q_1/q_{1rms}|$, the root mean square value q_{1rms} being 0.001 in the former case compared with 0.0013 for the latter. However, values of $|q_1| > 3q_{1rms}$ are significantly reduced.

It is clear from the results presented above that the wall oscillations act to change

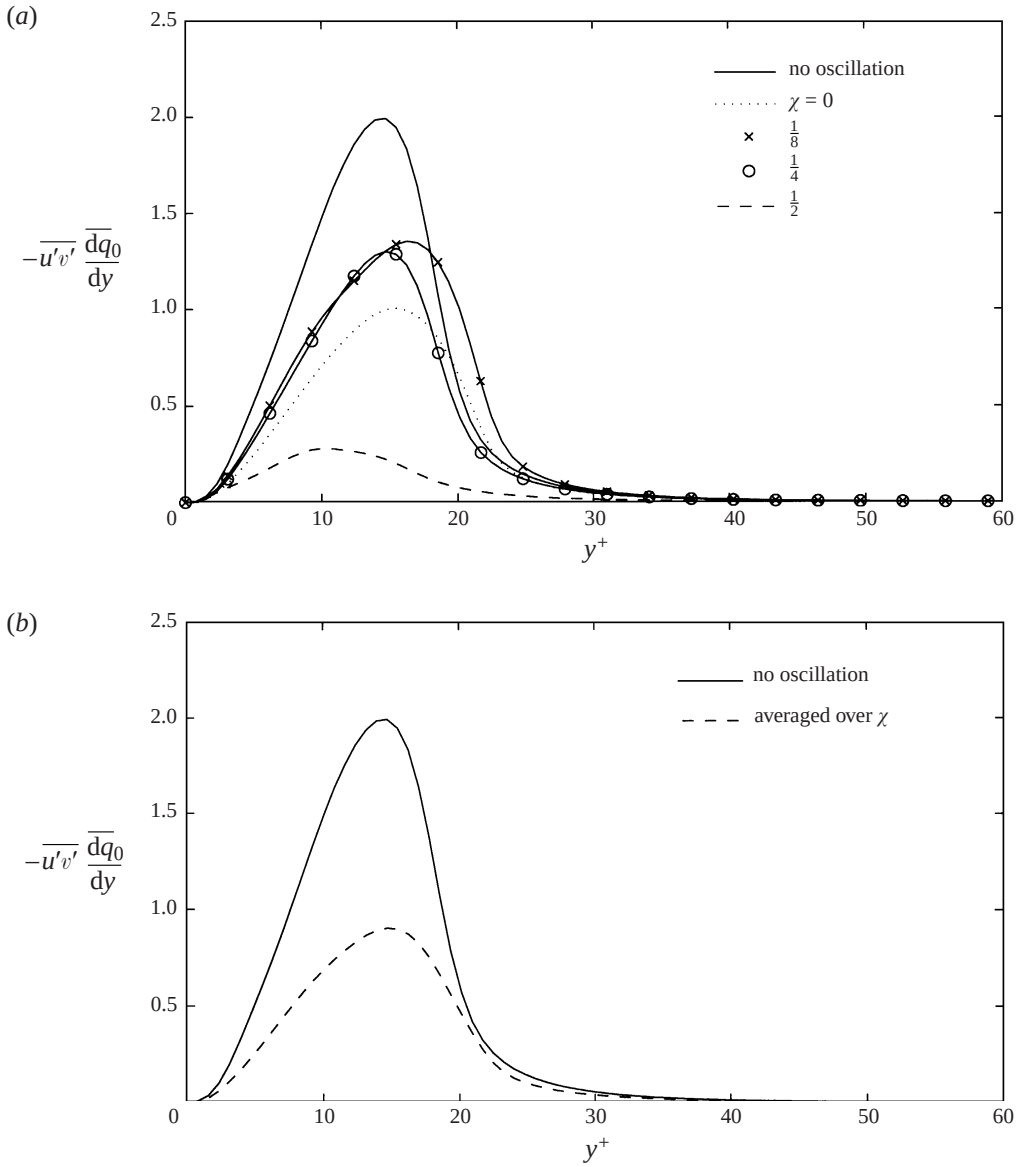

FIGURE 10. (*a*) Effect of spanwise oscillation on rate of energy production. The production rate in the case without oscillation is compared with that for the oscillatory ($T = 100$, $W_0 = 12$) case for different values of phase χ. The bar denotes average over z and t. $\Gamma = 300$, $a = 0.15$. (*b*) As in (*a*), but showing the comparison of the rate of production in the absence of oscillation with the corresponding rate, averaged over eight equally spaced phases χ, in the oscillatory case.

the coherent structure of turbulence in the inner layer of a boundary layer, in a way which can be anticipated by the present model. It is expected that the rate of occurrence of such structures will also be affected by the oscillation, in a way which cannot be predicted in the present consideration. The latter will require detailed consideration of the mechanism for turbulence production. Our results suggest that any such mechanism, if it is associated with the presence of coherent quasi-streamwise vortices, will be attenuated by the wall oscillations.

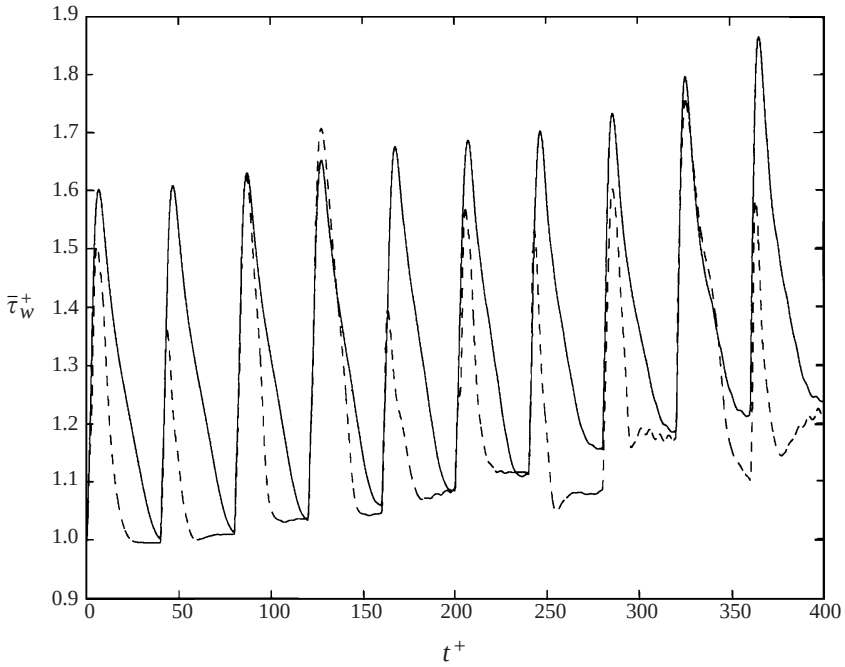

FIGURE 11. Effect of spanwise oscillation on skin friction, averaged over z, during a long simulation in which new structures are introduced in the flow at intervals of $t^+ = 40$. $\Gamma = 300$, $a = 0.15$: ——, without oscillation; - - - , spanwise oscillation with $T = 100$, $W_0 = 12$ and $\chi = 0$.

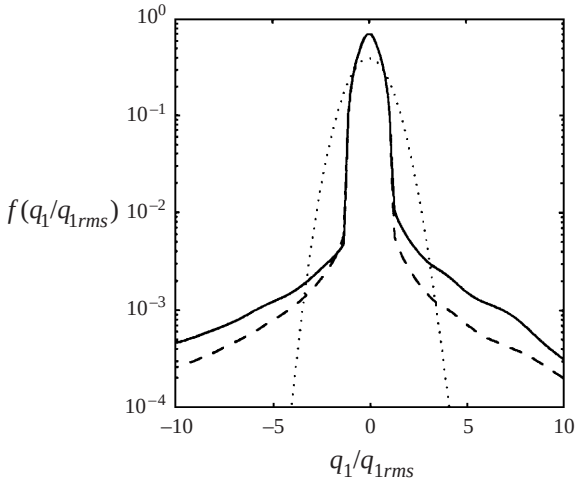

FIGURE 12. Influence of spanwise oscillation on the p.d.f. $f(q_1/q_{1\mathrm{rms}})$. The p.d.f.s $f^{(osc)}$ and $f^{(0)}$, for ——, the case in the absence of oscillation and - - -, the case with spanwise oscillation ($T = 100$, $W_0 = 12$ and averaged over χ) respectively, are compared with $\cdots$, the normalized Gaussian distribution.

4. Discussion

The present considerations elucidate the interaction between imposed spanwise wall oscillations and coherent quasi-streamwise vortical structures of the type found

in the near-wall region of a turbulent boundary layer. According to the model used here, these structures are the dominant features of the inner layer, together with the associated formation and maintenance of long streamwise streaks with low streamwise-speed momentum ejection in the middle and high streamwise-speed down-wash at each side. When a periodic, spanwise cross-flow, associated with the oscillatory motion of the surface beneath, is established in the surface layer, the coherent structures are deformed in a way which promotes their interaction with the rigid surface beneath, leading to their rapid annihilation. The severity of the process depends on the phase of the oscillation relative to the appearance of such structures near the wall and the rate of axial strain. The low-speed streaks are significantly distorted owing to mixing, by the oscillatory motion, of momentum associated with the low-speed ejection regions and that associated with the high-speed 'sweep' regions, resulting in a reduction in the rate of momentum convection normal to the wall. This in turn has a direct impact on the Reynolds stress and the skin friction. Over the time of the evolution of the structure ($t^+ \leqslant 40$), the reduction in skin friction is fairly independent of the period of oscillation, being around 10%, though a maximum reduction is obtained for the period $T^+ = 75$. This is consistent with the results of the DNS calculation in a channel (Jung *et al.* 1992), which show that for small times the skin friction reduction is around 10% for all periods considered; however, for $t^+ \gg 40$, when the present considerations no longer apply, the DNS calculation indicates occurrence of reductions of around 40% for $T^+ = 100$ whereas for $T^+ = 500$ a net increase in skin friction results, the actual value undergoing large oscillations. The present model shows that the wall oscillations significantly reduce the rate of production of kinetic energy. In this regard, the DNS calculation suggests that sustained oscillation results in suppression of coherent structures in the wall region. It is possible that sustained reduction in the rate of production of kinetic energy in the wall region, associated with the type of interaction studied here, has a significant effect on the long-term phenomena and consequently on the mechanism by which the coherent structures are generated in the wall region. Recent DNS work at low Reynolds numbers (see Hamilton, Kim & Waleffe 1995; Waleffe, 1995; Schoppa & Hussain, 1997; Jimenez & Pinelli 1998, for example) suggest that one such mechanism is a self-sustaining process in the wall region whereby the structures generate the low-speed streaks, decay and are regenerated through an instability of the flow associated with the streaks. The present considerations suggest that by promoting a rapid decay of the streamwise vortices and thereby weakening the low-speed streaks, the wall oscillations may be expected to profoundly attenuate such a self-sustaining process.

This work was supported by the Office of Naval Research under grant N00014-94-1-0453 (Program Manager: Dr Patrick Purtell) and by the National Science Foundation under grant BCS-9211-847.

REFERENCES

Bradshaw, P. & Pontikos, N. 1985 Measurements in the turbulent boundary layer on an 'infinite' swept wing. *J. Fluid Mech.* **159**, 105–130.

Choi, H. & Clayton, W. 1998 The mechanism of turbulent drag reduction with wall oscillation. *Proc. Intl Symp. on Seawater Drag Reduction, Newport, RI, USA, July, 1998.*

Choi, H., Moin, P. & Kim, J. 1994 Active turbulence control fror drag reduction in wall-bounded flows. *J. Fluid Mech.* **262**, 75–110.

Dhanak, M. R. & Dowling, A. P. 1995 On the pressure fluctuations induced by coherent vortex motion near a surface. *26th AIAA Fluid Dyn. Conf.* paper 95–2240.

Dhanak, M. R., Dowling, A. P. & Si, C. 1997 Coherent vortex model for surface pressure fluctuations induced by the wall region of a turbulent boundary layer. *Phys. Fluids* **9**, 2716–2731.

Frisch, U. 1995 *Turbulence*. Cambridge University Press.

Hamilton, J. M., Kim, J. & Waleffe, F. 1995 Regeneration mechanisms of near-wall turbulence structures. *J. Fluid Mech.* **287**, 317–348.

Jiménez, J. & Moin, P. 1991 The minimal flow unit in near-wall turbulence. *J. Fluid Mech.* **225**, 213–240.

Jiménez, J. & Pinelli, A. 1998 Turbulence near walls. *13th US National Congress of Applied Mechanics*, Gainesville, Florida. June, 1998.

Jung, W. J., Mangiavacchi, N. & Akhavan, R. 1992 Suppression of turbulence in wall-bounded flows by high-frequency spanwise oscillations. *Phys. Fluids* A **4**, 1605–1607.

Laadhari, F., Skandaji, L. & Morel, R. 1994 Turbulence reduction in a boundary layer by a local spanwise oscillating surface. *Phys. Fluids* **6**, 3218–3220.

Moin, P., Shih, T., Driver, D. & Mansour, N. 1990 Direct numerical simulation of three-dimensional turbulent boundary layer. *Phys. Fluids* A **2**, 1846.

Orlandi, P. & Jimenez, J. 1991 A model for bursting of near wall vortex structures in boundary layers. *8th Symposium on Turbulent Shear Flows*, Munich.

Orlandi, P. & Jimenez, J. 1994 On the generation of turbulent wall friction. *Phys. Fluids*, **6**, 634–641.

Pullin, D. I. & Saffman, P. G. 1998 Vortex dynamics in turbulence. *Ann. Rev. Fluid Mech.* **30**, 31–51.

Robinson, S. K. 1991 Coherent motions in the turbulent boundary layer. *Ann. Rev. Fluid Mech.* **23**, 601.

Schlichting, H. 1968 *Boundary-Layer Theory*, 6th edn. McGraw Hill.

Schoppa, W. & Hussain, F. 1997 Genesis and dynamics of coherent structures in near-wall turbulence. *Self-sustaining Mechanisms of Wall Turbulence* (ed. R. Panton) p. 385. Computational Mechanics Publications.

Spalart, P. R. 1988 Direct simulation of a turbulent boundary layer up to $Re_\theta = 1410$. *J. Fluid Mech.* **187**, 61–98.

Stuart, J. T. 1963 In *Laminar Boundary Layers* (ed. L. Rosenhead). Dover.

Waleffe, F. 1995 Hydrodynamic stability and turbulence: beyond transients to a self-sustaining process. *Stud. Appl. Maths* **95**, 319.